High-resolution non-line-of-sight imaging via polarization differential correlography: Supplemental Material

1. SYSTEM SETUP

The PDC-NLOS imaging system setup consists of incident laser source, collimating lens, steering, the relay wall, DMD, polarization camera and its focusing lens. The system setup is shown in Fig. S1.

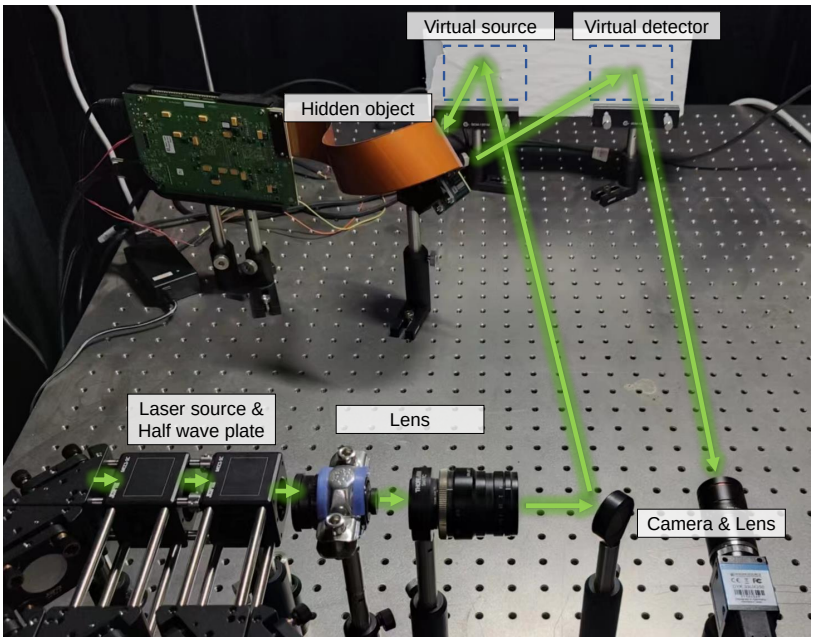

Fig. S1. Practical system setup for PDC-NLOS imaging method.

The wavelength of the incident Laser source is set to 532 nm. The polarization camera contains a microlens array with four polarization angles to achieve polarization imaging.

2. FAR-FIELD CONDITION IN THE FORWARD PROCESS MODELING

In the forward process modeling, Eq. 1 describes the light field at the VS and does not require a far-field condition. The propagation from the VS to the hidden object is governed by Eq. 2, which includes the Fresnel diffraction formulation and does not assume a far-field condition. Similarly, the camera with a lens focused on the relay wall does not require a far-field condition. However, the propagation from the hidden object to the VD does need to satisfy the far-field condition, as this is essential for the validity of the far-field approximation used in Eq. 3:

$$\mathbf{E_{VD}}\left(x,y\right) = c_1 \mathcal{F}\left[\mathbf{E_O}\left(x,y\right)\right] = c_1 \sum_{\theta_n=0}^{2\pi} \mathbf{E_{O_p}}\left(x,y;\theta_n\right). \tag{S1}$$

According to the citation [1], for the relationship to be Fourier transform, the distance between the object and the VD should be equal to the far field distance which is given by,

$$Z_{far-field} = \frac{2D_{obj}^2}{\lambda}, \tag{S2}$$

Where D_{obj} is the size of the object.Since the object in our experiment is not illuminated by a laser beam, the far field distance is no longer given by the above expression. The far field distance is given by the geometric mean of the coherence area of the speckle field at the object plane and area of the object A_{obj} which is a much smaller distance [2].

$$Z_{far-field} = \frac{2\sqrt{A_c A_{obj}}}{\lambda}. \tag{S3}$$

According to the citation [3], A_c can be expressed by

$$A_c = \frac{(\lambda z)^2}{A_{speckle}}, \tag{S4}$$

where $A_{speckle} = L^2$ is the average size of the speckle, L is width of the scattering area.

Then Eq. S3 can be expressed as

$$Z_{far-field} = \frac{2zD_{obj}}{L}. \tag{S5}$$

Substitute $D_{obj} = 10\ mm$, $Z_{vs2obj} = 300\ mm$, the diameter of the scattering region on the VS is about 20 mm, and the distance from the object to the VD should be greater than 300 mm. In the experiment system, the value of the object to the VD is set to approximately 400 mm, which satisfies the far-field condition.

3. COHERENT REPRESENTATION OF POLARIZATION SPECKLE INTENSITY

The coherence matrix $\mathbf{J}$ of the $\mathbf{E_{VS}}$ can be expressed as

$$\mathbf{J} = \begin{bmatrix} \langle E_x^2 \rangle & \langle E_x E_y \exp(j\delta) \rangle \\ \langle E_x E_y \exp(-j\delta) \rangle & \langle E_y^2 \rangle \end{bmatrix}, \tag{S6}$$

where δ is the phase difference between the horizontal and vertical components. Since the incident light is a quasi-monochromatic plane wave, $\delta = m\pi, m = 0, \pm 1, \pm 2 \cdots$. Eq. S6 can be written as

$$\mathbf{J} = \begin{bmatrix} \langle E_x^2 \rangle & \langle E_x E_y \rangle \\ \langle E_x E_y \rangle & \langle E_y^2 \rangle \end{bmatrix}. \tag{S7}$$

Considering the speckle field observed at θ, the complex amplitude $\mathbf{E_p}$ can be expressed as

$$\begin{aligned} \mathbf{E_p}(x, y; \theta) = &\left[\cos^2\theta \cdot E_x + \sin\theta\cos\theta \cdot E_y\right] \vec{\mathbf{x}} \\ &+ \left[\sin\theta\cos\theta \cdot E_x + \cos^2\theta \cdot E_y\right] \vec{\mathbf{y}}, \end{aligned} \tag{S8}$$

and the intensity I_p can be expressed as

$$\begin{aligned} I_p(x, y; \theta) = &\cos^2\theta \cdot J_{xx} + \sin\theta\cos\theta \cdot J_{xy} + \sin\theta\cos\theta \cdot J_{yx} \\ &+ \sin^2\theta \cdot J_{yy}, \end{aligned} \tag{S9}$$

where J_{ij} is the (i, j) term of the coherence matrix $\mathbf{J}$.

Thus, the correlation coefficient of the speckles at the observation angles θ_1 and θ_2 can be expressed as

$$\begin{aligned} C(\theta_1, \theta_2) = &\frac{\langle \Delta I(\theta_1) \Delta I(\theta_2) \rangle}{\sigma(\theta_1)\sigma(\theta_2)} \\ = &\frac{\cos\theta_1\cos\theta_2 + \zeta\sin\theta_1\sin\theta_2}{\left(\cos^2\theta_1 + \zeta\sin^2\theta_1\right)\left(\cos^2\theta_2 + \zeta\sin^2\theta_2\right)}, \end{aligned} \tag{S10}$$

4. IMAGING EXPERIMENTS WITH DIFFERENT NUMBER OF POLARIZATION DIFFERENTIAL SPECKLES USED

As shown in Fig. S2, the autocorrelation has valuable contrast and structural integrity when using a complete set of 4 polarization differential speckles (0°, 45°, 90° and 135°) to encode the hidden object in a single shot. The structure of the reconstruction result is clear and complete, with a Structural Similarity Index Measure (SSIM) of 0.7405, which quantifies the similarity between the reconstructed and ground-truth images. When the number of polarization differential speckles is reduced to 3 (0°, 45° and 90°), N corresponding to Eq. 7 and Eq. 8 will be reduced to 3/4 of the original situation, the contrast of the autocorrelation estimate is reduced, and the structure is intact. The reconstruction result is noisy on the complete structure, with an SSIM of 0.6713. When the number of polarization differential speckles reaches 2 (0° and 45° or 0° and 90°), the contrast of the autocorrelation estimate continues to decrease, and the structure begins to defect. The reconstruction result is missing some structures and has reduced contrast, with SSIM values of 0.6102 and 0.6231, respectively.

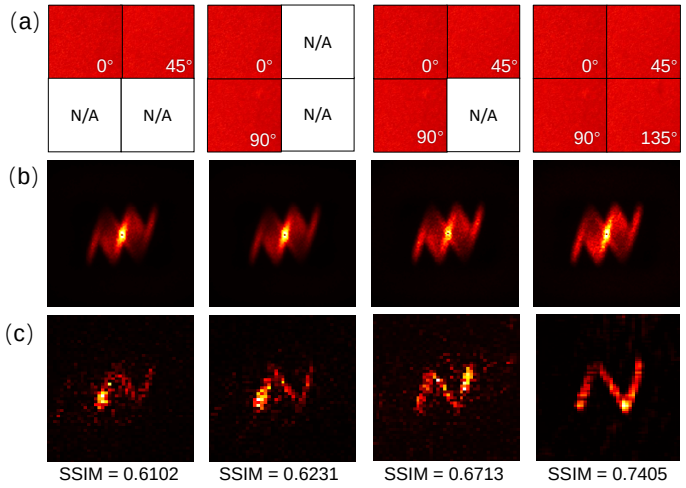

Fig. S2. Imaging experiment on the number of polarization differential speckles. (a) Polarization differential speckles were used. (b) autocorrelation calculated by PDC-NLOS. (c) reconstruction of the hidden object.

It is worth noting that there is not much difference in the reconstruction results obtained by using 2 polarization differential speckles at 0° and 45° and using 2 polarization differential speckles at 0° and 90°. This is because polarization differential correlography can obtain stable difference in polarized speckles beyond the correlation range. Combined with the designed single-shot polarized speckle illumination strategy and an intensity calibration method, the stability of the reconstruction is guaranteed.

5. IMAGING EXPERIMENTS WITH DIFFERENT KIND OF RELAY WALLS

In this section we use different relay wall materials to verify the generalization ability of PDC-NLOS in different scenarios. We used common latex paint, paper and diamond grade retrorefective material to make relay walls. It is noted that the uneven diffusion of the VD can affect the quality of secondary speckle acquisition. When using the relay wall made of diamond grade retrorefective material for the experiment, we only replaced VS, and the VD material still used latex paint with better uniformity.

As shown in Fig. S3, the imaging results of using three materials as the intermediate surface of PDC-NLOS. Latex paint and paper can produce polarized speckle illumination with high contrast and clear structure because their surfaces are uniform and have no obvious structure. Therefore, the estimated auto-correlation structure is complete and has high contrast, and a available reconstruction can be solved. However, diamond grade retrorefective material produces a polarized speckle illumination with low contrast and uneven structure due to its obvious surface structure. The estimated auto-correlation structure is partially lost, the contrast is low, and the reconstruction is low in accuracy and incomplete.

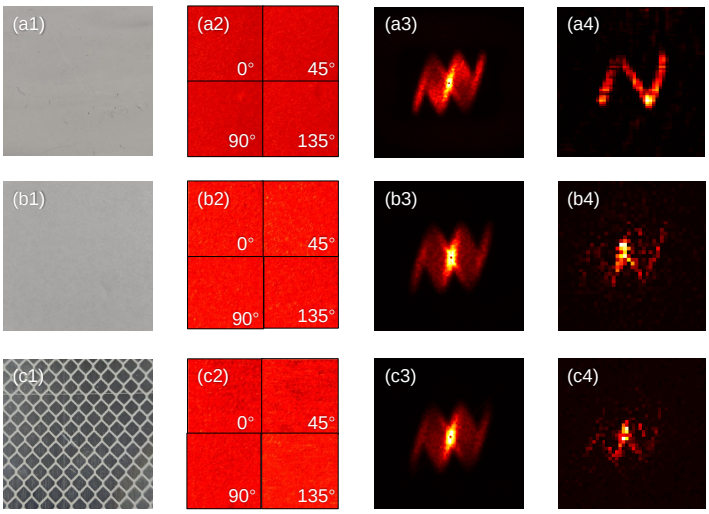

Fig. S3. Results of imaging experiments with different relay surface materials. (a1) Relay wall made of latex paint. (b1) Paper relay wall, (c1) relay wall made of diamond grade retrorefective material, (a2-c2) captured polarization differential speckles, (a3-c3) auto-correlation calculated by PDC-NLOS, (a4-c4) reconstruction of the hidden object.

Considering the efficiency of light energy transmission, diamond grade retrorefective material has the highest reflectivity, the camera exposure time is short, and faster acquisition can be performed. Paper has the lowest reflectivity among the three materials and requires the longest acquisition time. In conclusion, PDC-NLOS has the best imaging effect on the most common latex paint wall. Usable results can also be obtained on other materials due to the coding redundancy of polarized speckle illumination.

Furthermore, to address the impact of uneven diffusion from the VD on the quality of secondary speckle acquisition, future work will focus on incorporating the BRDF of the relay wall surface into the image reconstruction process to enhance the method's robustness and applicability.

REFERENCES

1. A. Viswanath, "Indirect imaging using computational imaging techniques," Electr. Eng. Theses Diss. 17. (2018).
2. J. W. Goodman, "Statistical properties of laser speckle patterns," in *Laser speckle and related phenomena*, (Springer, 1975), pp. 9–75.
3. J. W. Goodman, *Speckle phenomena in optics: theory and applications* (Roberts and Company Publishers, 2007).